Draft version May 8, 2020
Typeset using LaTeX **preprint** style in AASTeX62

Empirical Dust Models

ChangHoon Hahn[1,2,*] and IQ Collaboratory

[1] *Lawrence Berkeley National Laboratory, 1 Cyclotron Rd, Berkeley CA 94720, USA*
[2] *Berkeley Center for Cosmological Physics, University of California, Berkeley CA 94720, USA*

(Dated: DRAFT --- fa37c03 --- 2020-05-07 --- NOT READY FOR DISTRIBUTION)

ABSTRACT

dust

Keywords: keyword1 – keyword2 – keyword3

1. INTRODUCTION

dust is important because....

assumptions on the attenuation curve can dramatically impact the physical properties inferred from SED fitting (*e.g.* Kriek & Conroy 2013; **?**; **?**; Salim & Narayanan 2020).

motivation for an empirical dust attenuation model

attenuation vs extinction. While extinction curves have been derived from observations and theoretically, it's not easy to map this to attenuation curves. Attenuation curves are a product of complicated empirical processes since it accounts for light that gets scattered and star light that is not obscured

This makes modeling them in a complete physically motivated method expensive. People have done it Narayanan et al. (2018); Trayford et al. (2020). some detail about the radiative transfer method and such. But besides being expensive they have to make a number of assumptions anyway. e.g. Narayanan et al. (2018) assumes a fixed extinction curve.

Moreover, because the radiative transfer method is expensive it's hard to compare many different simulations. Not only that, observables generated from simulations that take into radative transfer dust models complicates simulation to simulation comparisons. Because you're simultaneously comparing the galaxy formation prescription and all the dust prescription.

Instead, we present a framework using flexible dust empirical models that paints attenuation curves onto galaxies. describe at a high level how we are parameterizing DEMs

talk about the advantages: extremely flexible so it can encompass the wide variety of attenuation curves found in radiative transfer, easy to correlate the attenuation curve with galaxy properties.

Also DEMs make it possible to statistically apply attenuation curves for large galaxy population. Putting this ontop of simulations, we can use them to generate observables and compare them to

* hahn.changhoon@gmail.com

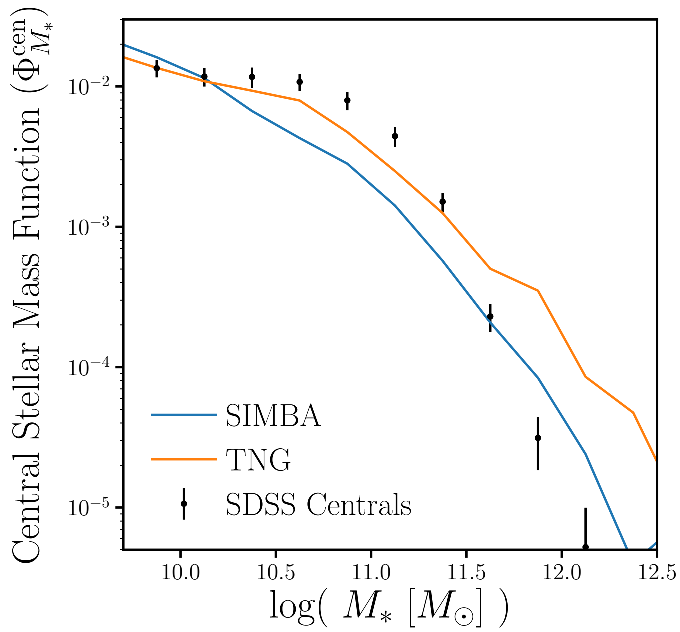

Figure 1. The stellar mass functions of central galaxies from the SIMBA (orange) and TNG (blue) simulations compared to the central SMF of SDSS (Section 2.5). The uncertainties for the SDSS SMF is derived using jackknife resampling.

observations to constrain the DEM. This framework allows us to learn about attenuation curves given a model for galaxy formation.

The other way around also works. If you don't care about dust at all, DEM provides a framework to easily marginalize over dust attenuation and treat dust as a nuisance parameter.

In this paper, we do above for multiple simulations.

Starkenburg et la. in prep will use this framework to marginalize over dust and compare galaxy populations predicted by multiple simulations .

2. DATA

2.1. *Illustris TNG*

describe what galaxy properties (SFH, ZH, etc) are available TODO

2.2. *SIMBA*

describe what galaxy properties (SFH, ZH, etc) are available TODO

2.3. *Spectral Energy Distributions*

describe how the SED is generated using the SFH and ZHs TODO

2.4. *Forward Modeling SDSS Photometry and Spectra*

2.5. *SDSS DR7 Central Galaxies*

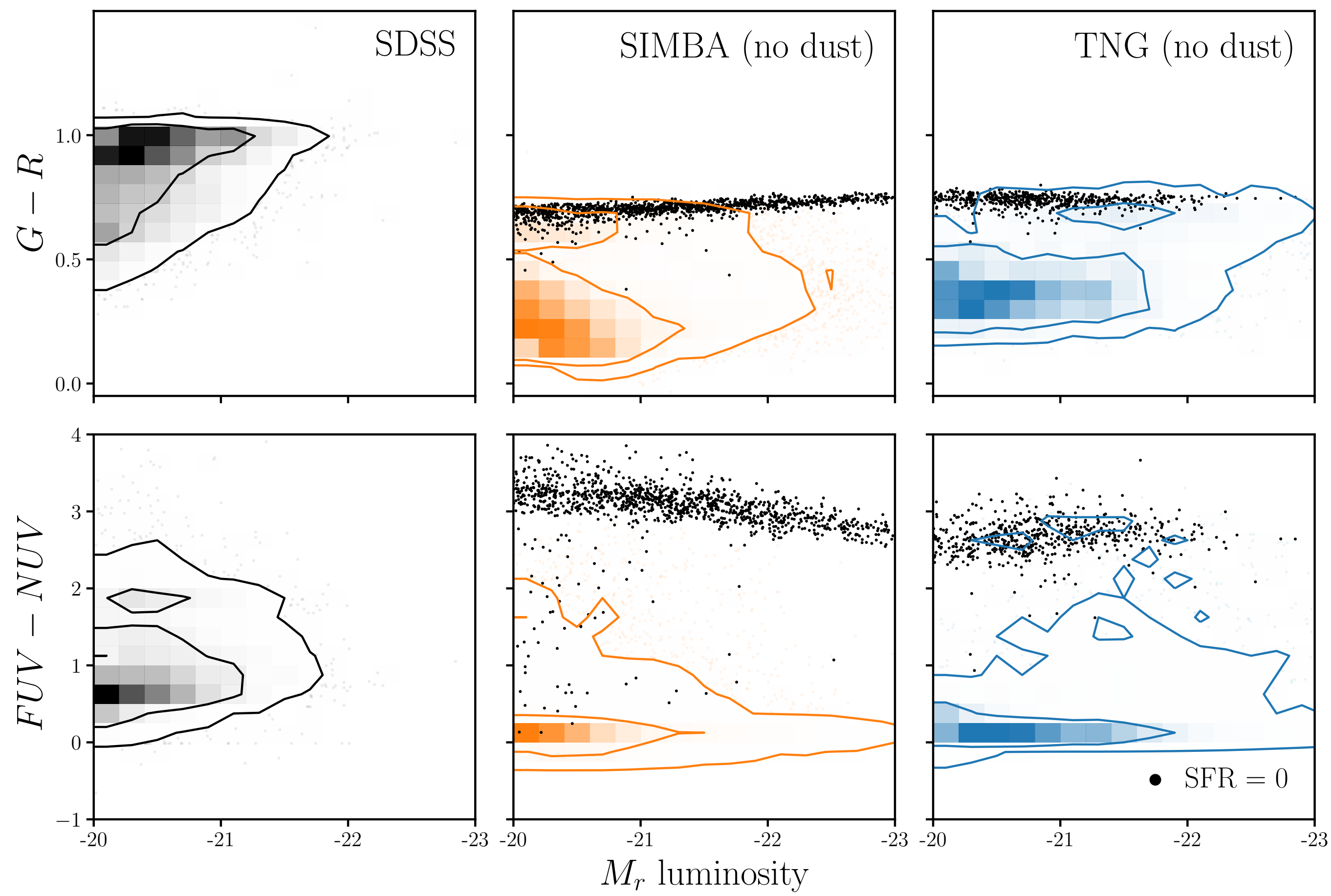

Figure 2.

We compare the simulations above to central galaxies sample from the Tinker et al. (2011) SDSS group catalog. The Tinker et al. (2011) group catalog, first, selects volume-limited sample of galaxies at $z \approx 0.04$ with $M_r < -18$ and complete above $M_* > 10^{9.4}h^{-2}M_\odot$ from the NYU Value-Added Galaxy Catalog (VAGC; Blanton et al. 2005) of SDSS DR7 (Abazajian et al. 2009). The stellar masses are estimated using the `kcorrect` code (Blanton & Roweis 2007) assuming a Chabrier (2003) initial mass function.

Central galaxies are then identified using a halo-based group finder that uses the abundance matching ansatz to iteratively assign halo masses to groups. Every group contains one central galaxy, which by definition is the most massive, and a group can contain ≥ 0 satellites. As with any group finder, galaxies are misassigned due to projection effects and redshift space distortions; however, the central galaxy sample has a purity of $\sim$90% and completeness of $\sim$95% (Tinker et al. 2018).

In Figure 1, we present the stellar mass function (SMF) of our SDSS central galaxy sample along with central galaxy SMFs of the SIMBA (orange) and TNG (blue) simulations. The uncertainties for the SDSS SMF are derived from jackknife resampling. Although we present the SMFs for reference, we do not use stellar masses throughout the paper since they are inconsistently defined among simulations and observations. Instead, we compare between the simulations and SDSS using luminosity, M_r, which we consistently forward model and measure in the simulations. In these comparisons, we restrict ourselves to galaxies brighter than $M_r < -20$, where our SDSS central galaxy sample is complete.

3. DUST EMPIRICAL MODELING

3.1. *Fiducial DEM*

motivation for the DEM model TODO

We begin by defining the dust attenuation curve $A(\lambda)$ as

$$F_o(\lambda) = F_i(\lambda) 10^{-0.4 A(\lambda)} \tag{1}$$

where F_o is the observed flux and F_i is the intrinsic flux. We normalize the attenuation at the V band,

$$A(\lambda) = A_V \frac{k(\lambda)}{k_V}. \tag{2}$$

For the normalization of the attenuation curve, A_V, we use the slab model from Somerville & Primack (1999); Somerville et al. (2012). In the slab model the amplitude of attuenuation depends on the inclination angle, i, and the optical depth, τ_V:

$$A_V = -2.5 \log \left[\frac{1 - e^{-\tau_V \sec i}}{\tau_V \sec i} \right] \tag{3}$$

justification of why this is enough. We sample i uniformly. TODO

Recently, Salim & Narayanan (2020) find significant dependence in A_V on both M_* and SFR. We include this dependence through τ_V, which we flexibly parameterize as

$$\tau_V(M_*, \mathrm{SFR}) = m_{\tau,1} \log \left(\frac{M_*}{10^{10} M_\odot} \right) + m_{\tau,2} \log \mathrm{SFR} + c_\tau. \tag{4}$$

Next, for the wavelength dependence of the attenuation curve, we use $k(\lambda)$ from Noll et al. (2009):

$$k(\lambda) = (k_{\mathrm{Cal}}(\lambda) + D(\lambda)) \left(\frac{\lambda}{\lambda_V} \right)^\delta. \tag{5}$$

Here $k_{\mathrm{Cal}}(\lambda)$ is the Calzetti (2001) curve:

$$k_{\mathrm{Cal}}(\lambda) = \begin{cases} 2.659(-1.857 + 1.040/\lambda) + R_V, & 6300\mathring{A} \le \lambda \le 22000\mathring{A} \\ 2.659(-2.156 + 1.509/\lambda - 0.198/\lambda^2 + 0.011/\lambda^3) + R_V & 1200\mathring{A} \le \lambda \le 6300\mathring{A} \end{cases}$$

where λ_V is the V band wavelength. δ, the slope of the attenuation curve. also correlates with galaxy properties. So we parameterize δ and

$$\delta(M_*, \mathrm{SFR}) = m_{\delta,2} \log \left(\frac{M_*}{10^{10} M_\odot} \right) + m_{\delta,2} \log \mathrm{SFR} + c_\delta \tag{6}$$

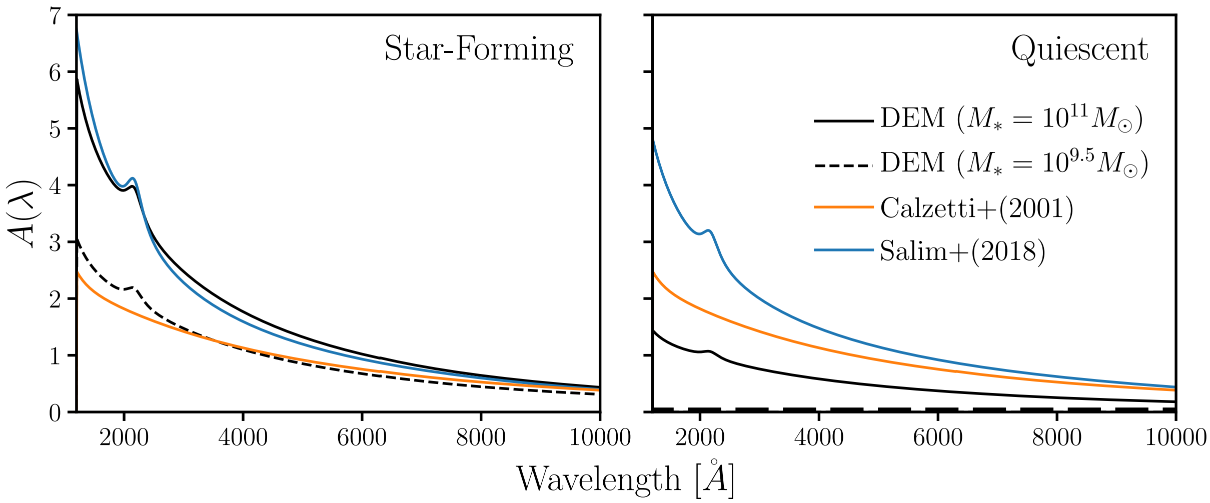

Figure 3. comparison of fiducial DEM to attenuation curve in the literature.

$D(\lambda)$ is the UV dust bump, which we parameter using the standard Lorentzian-like Drude profile:

$$D(\lambda) = \frac{E_b(\lambda\Delta\lambda)^2}{(\lambda^2 - \lambda_0^2)^2 + (\lambda\Delta\lambda)^2} \tag{7}$$

where λ_0, $\Delta\lambda$, and E_b are the central wavelength, FWHM, and strength of the bump, respecitvely. In our DEM, we assume fixed $\lambda_0 = 2175\mathring{A}$ and $\Delta\lambda = 350\mathring{A}$.

Kriek & Conroy (2013) and Tress et al. (2018) found evidence that E_b correlates with the slope of the attenuation curve for star-forming galaxies $z \sim 2$. This was dependence was confirmed with simulations in **?**. E_b:

$$E_b = m_E\ \delta + c_E \tag{8}$$

We also split the attenuation on the star light and nebular emission

$$F_o(\lambda) = F_i^{\rm star}(\lambda)10^{-0.4A(\lambda)} + F_i^{\rm neb}(\lambda)10^{-0.4A_{\rm neb}(\lambda)} \tag{9}$$

where we parameterize

$$A_{\rm neb}(\lambda) = f_{\rm neb}A(\lambda) \tag{10}$$

mention of how we treat SFR = 0 galaxies TODO

3.2. *Beyond the Slab DEM*

A major assumption of our fiducial DEM is that we sample the amplitude of attenuation from the slab model. The slab model makes a strong simplifying assumption that the dust in galaxies details. TODO sentence or two about how we know the slab model doesn't work. TODO

Furthermore, the slab model predicts A_V distribution significantly different than A_V distributions measured from observations. In Figure **??**, we compare the A_V distribution predicted by the slab model for τ_V = to the A_V distribution of SDSS galaxies from **?**. The comparison clearly reveals

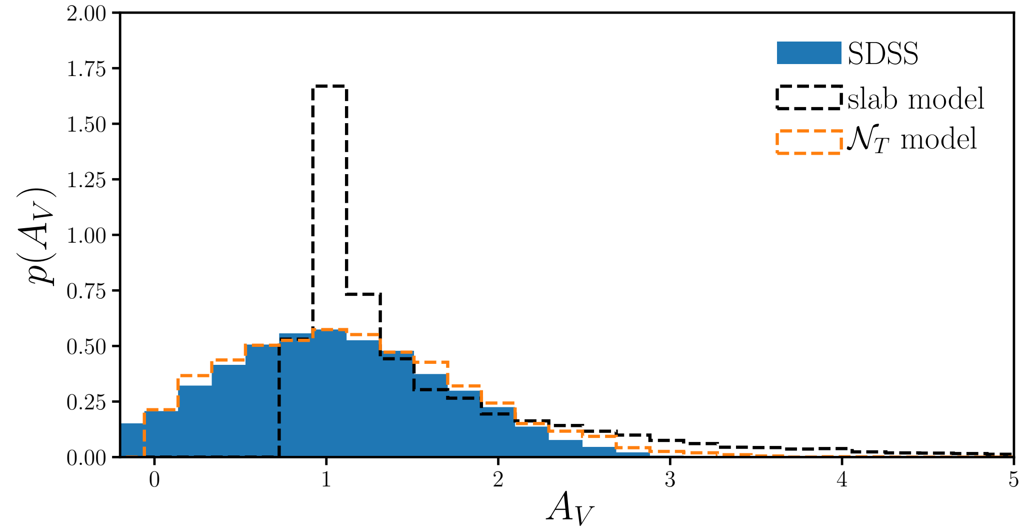

Figure 4. Comparisons of A_V distribution from slab model (Eq. **??**, truncated normal model (Eq. **??**, and SDSS SF galaxies.

the discrepancy between the SDSS A_V distribution and the slab model prediction. The slab model predicts a sharp cutoff at lower A_V end of the distribution, which is not found in observables. The SDSS A_V measurements can be negative in **?** because .... TODO

To ensure that our results do not depend significantly on the slab model, we implement a more flexible alternative model for sampling A_V based on a truncated normal distribution:

$$A_V \sim \mathcal{N}_T(\mu_{A_V}, \sigma_{A_V}) = \frac{\mathcal{N}(\mu_{A_V}, \sigma_{A_V})}{1 - \Phi\left(-\frac{\mu_{A_V}}{\sigma_{A_V}}\right)}. \tag{11}$$

$\mathcal{N}$ is the standard normal distribution and Φ is the cumulative distribution function of the standard normal distribution function. $\Phi(x) = \frac{1}{2}(1 + \mathrm{erf}(x/\sqrt{2})$. μ_{A_V} and σ_{A_V} are the mean and variance of the truncated normal distribution. There TODO

3.3. *Likelihood-Free Inference*

Approximate Bayesian Computation with Population Monte Carlo Hahn et al. (2017),
discussion of observables and distance metric Ishida et al. (2015)
Paragraph on the priors we choose.

4. RESULTS

- There isn't a whole lot of flexibility for SFR=0 galaxies predicted by simulations and they do not agree well with observations A.

5. SUMMARY

ACKNOWLEDGEMENTS

Table 1. Free Parameters of the Dust Empirical Models separate section for slab model vs tnorm model

Parameter	Definition
$m_{\tau,1}$	Slope of the $\log M_*$ dependence of optical depth, τ_V
$m_{\tau,2}$	Slope of the $\log \mathrm{SFR}$ dependence of optical depth, τ_V
c_τ	amplitude of the optical depth, τ_V
$m_{\delta,1}$	Slope of the $\log M_*$ dependence of the attenuation curve slope, δ
$m_{\delta,2}$	Slope of the $\log \mathrm{SFR}$ dependence of the attenuation curve slope, δ
c_δ	amplitude of the attenuation curve slope, δ
m_E	slope of the δ dependence of UV dust bump strength, E_b
c_E	amplitude of UV dust bump strength, δ
$f_{\rm neb}$	fraction of nebular attenuation curve

It's a pleasure to thank ... This material is based upon work supported by the U.S. Department of Energy, Office of Science, Office of High Energy Physics, under contract No. DE-AC02-05CH11231. This project used resources of the National Energy Research Scientific Computing Center, a DOE Office of Science User Facility supported by the Office of Science of the U.S. Department of Energy under Contract No. DE-AC02-05CH11231.

APPENDIX

A. RESOLUTION EFFECTS

Figure demonstrating imprint SFR=0 leave on the observable space and how we deal with them so we can ignore them...

REFERENCES

Abazajian K. N., et al., 2009, The Astrophysical Journal Supplement Series, 182, 543

Blanton M. R., Roweis S., 2007, The Astronomical Journal, 133, 734

Blanton M. R., et al., 2005, The Astronomical Journal, 129, 2562

Calzetti D., 2001, New Astronomy Reviews, 45, 601

Chabrier G., 2003, Publications of the Astronomical Society of the Pacific, 115, 763

Hahn C., Vakili M., Walsh K., Hearin A. P., Hogg D. W., Campbell D., 2017, Monthly Notices of the Royal Astronomical Society, 469, 2791

Ishida E. E. O., et al., 2015, Astronomy and Computing, 13, 1

Kriek M., Conroy C., 2013, The Astrophysical Journal Letters, 775, L16

Narayanan D., Conroy C., Davé R., Johnson B. D., Popping G., 2018, The Astrophysical Journal, 869, 70

Noll S., Burgarella D., Giovannoli E., Buat V., Marcillac D., Muñoz-Mateos J. C., 2009, Astronomy and Astrophysics, 507, 1793

Salim S., Narayanan D., 2020, arXiv:2001.03181 [astro-ph]

Somerville R. S., Primack J. R., 1999, Monthly Notices of the Royal Astronomical Society, 310, 1087

Somerville R. S., Gilmore R. C., Primack J. R., Domínguez A., 2012, Monthly Notices of the Royal Astronomical Society, 423, 1992

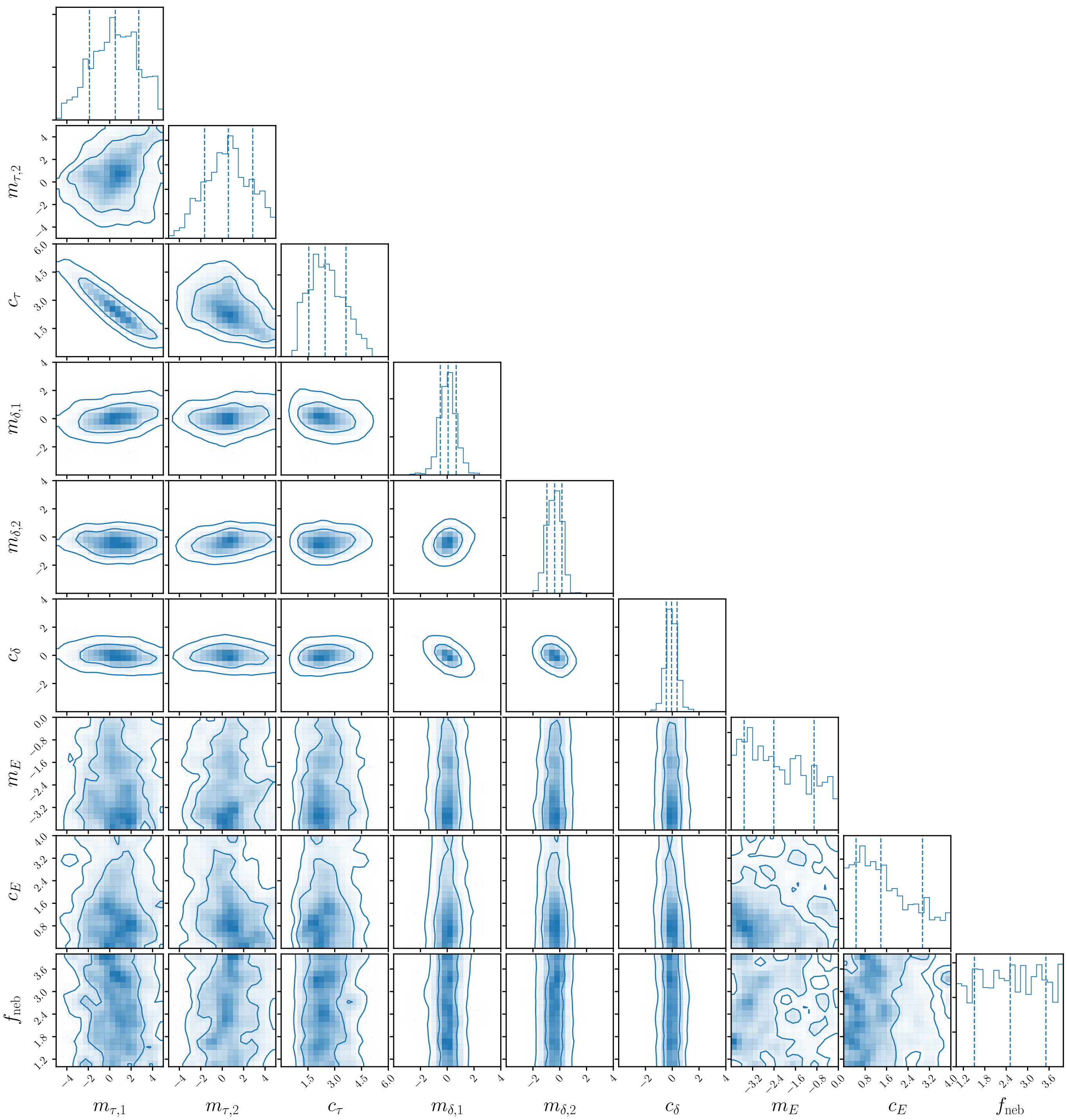

Figure 5. Posterior of the DEM parameters.

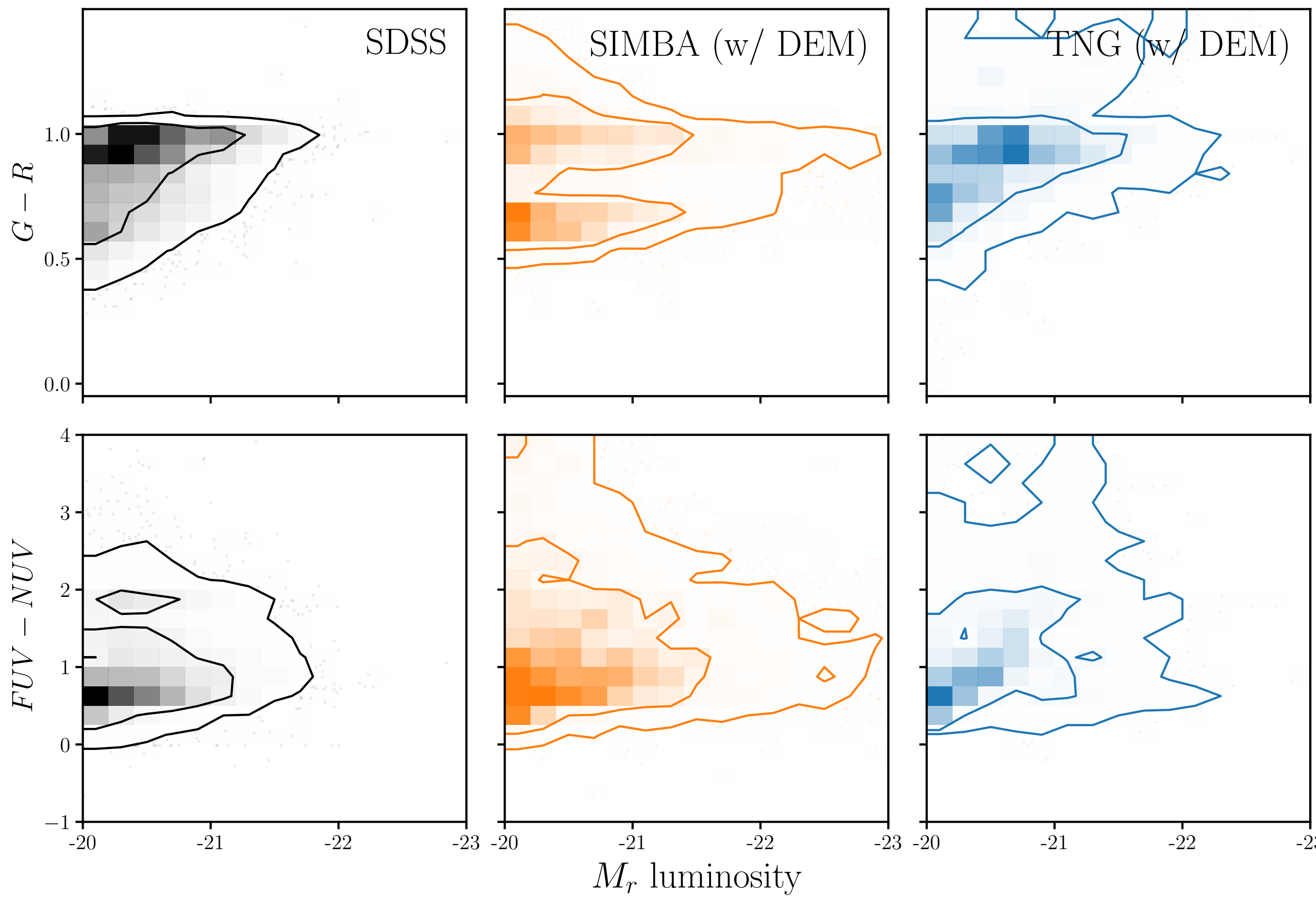

Figure 6. Comparison of the observables predicted by the simulations with the posterior DEM.

Tinker J., Wetzel A., Conroy C., 2011, preprint, 1107, arXiv:1107.5046

Tinker J. L., Hahn C., Mao Y.-Y., Wetzel A. R., Conroy C., 2018, Monthly Notices of the Royal Astronomical Society, 477, 935

Trayford J. W., Lagos C. d. P., Robotham A. S. G., Obreschkow D., 2020, Monthly Notices of the Royal Astronomical Society, 491, 3937

Tress M., et al., 2018, Monthly Notices of the Royal Astronomical Society, 475, 2363